Weierstraß-Institut
für Angewandte Analysis und Stochastik

im Forschungsverbund Berlin e.V.

Preprint ISSN 0946 – 8633

Finite Element Method for Epitaxial Growth with thermodynamic boundary conditions

Eberhard Bänsch[1], Frank Haußer[2] , Axel Voigt[2]

submitted: 12th January 2004

[1] Weierstrass Institute for
Applied Analysis and Stochastics
Mohrenstrasse 39
10117 Berlin
and Freie Universität Berlin
Germany
e-mail: baensch@wias-berlin.de

[2] Research Center caesar
Ludwig-Erhard-Allee 2
53175 Bonn
Germany
e-mail: hausser@caesar.de
voigt@caesar.de

No. 873
Berlin 2003

2000 *Mathematics Subject Classification.* 35Q99, 35R35, 65N30, 65Z05, 74S05.

Key words and phrases. epitaxial growth, island dynamics, free or moving boundary problem, adatom diffusion, surface diffusion, mean curvature flow, Gibbs-Thomson, finite elements, adaptivity, front tracking.

Edited by
Weierstraß-Institut für Angewandte Analysis und Stochastik (WIAS)
Mohrenstraße 39
10117 Berlin
Germany

Fax: + 49 30 2044975
E-Mail: preprint@wias-berlin.de
World Wide Web: http://www.wias-berlin.de/

FINITE ELEMENT METHOD FOR EPITAXIAL GROWTH WITH THERMODYNAMIC BOUNDARY CONDITIONS

EBERHARD BÄNSCH, FRANK HAUSSER, AND AXEL VOIGT

Abstract. We develop an adaptive finite element method for island dynamics in epitaxial growth. We study a step-flow model, which consists of an adatom (adsorbed atom) diffusion equation on terraces of different height; thermodynamic boundary conditions on terrace boundaries including anisotropic line tension; and the normal velocity law for the motion of such boundaries determined by a two-sided flux, together with the one-dimensional (possibly anisotropic) "surface" diffusion of edge-adatoms along the step-edges. The problem is solved using two independent meshes: a two-dimensional mesh for the adatom diffusion and a one-dimensional mesh for the boundary evolution. A penalty method is used in order to incorporate the boundary conditions. The evolution of the terrace boundaries includes both the weighted/anisotropic mean curvature flow and the weighted/anisotropic surface diffusion. Its governing equation is solved by a semi-implicit front-tracking method using parametric finite elements.

1. Introduction

A framework for finite element simulations of epitaxial growth was recently developed by the authors in [1]. Here we will extend the methods to treat also thermodynamic boundary conditions and anisotropic growth.

Epitaxial growth is a modern technology of growing single crystal films that inherit atomic structures from substrates. There are various kinds of models for epitaxial growth, among them are the step-flow models of Burton-Cabrera-Frank (BCF) type, cf. [3, 4, 5, 8, 9, 11]. Here the description of the growth is continuous in the lateral directions but discrete in the growth direction. The model is essentially a free boundary problem that consists of a diffusion equation for the adatom density on islands, boundary conditions for the moving island boundaries and an evolution equation for the island boundaries. If the attachment/detachment processes at the island boundaries are fast compared to the adatom diffusion on the islands (*diffusion limited growth*), the island boundaries act as perfect sinks for the adatoms. This is modeled by thermodynamic boundary conditions. As in [1], in developing our finite element method, we naturally divide our underlying problem into two parts: the adatom diffusion and the boundary evolution:

1991 *Mathematics Subject Classification.* 35Q99, 35R35, 65N30, 65Z05, 74S05.

Key words and phrases. Epitaxial growth, island dynamics, free or moving boundary problem, adatom diffusion, surface diffusion, mean curvature flow, Gibbs-Thomson, finite elements, adaptivity, front tracking.

1. We derive a weak formulation for the time-dependent diffusion equation. To avoid the complexity of evaluating the adatom fluxes at the boundaries, boundary conditions are incorporated by a penalty method. The resulting equation is discretized using the linear finite element method. The resulting linear system is symmetric positive definite, and is solved by the conjugate gradient method.
2. The geometric motion of the island boundaries includes both the mean curvature flow and the surface diffusion. It is treated in a variational formulation utilizing the curvature vector, and discretized by a semi-implicit front-tracking method using parametric finite elements. This method is adapted with modification from [1, 2, 7] and extended to also handle anisotropy.

To obtain satisfactory computational results, meshes with sufficiently fine resolutions are needed for both the adatom diffusion equation and the boundary evolution equation. Thus, it is indispensable to use adaptivity in order for the method to be efficient. We use simple error indicators within an h-adaptive method to locally increase the spatial resolution.

We apply our method to the following test problems: a) a pure geometric problem of the evolution of the boundaries that is governed by either the motion by weighted/anisotropic mean curvature or the motion by weighted/anisotropic surface diffusion. Our numerical results show the expected "convergence" to the Wulff shape; b) the stability of a growing circular island. This problem has been analyzed rigorously in [10]. Our method yields numerical results that are in agreement with the theory. Besides these test problems, the method is used to study the influence of surface diffusion on anisotropic growth of a single island; Furthermore, we present simulations of the isotropic evolution of a single "wedding cake" and the anisotropic evolution of several islands on a substrate. At the present stage, our method is not capable of handling topological changes of the moving boundaries arising from nucleation and coalescence of adatom islands.

In Section 2, we describe the problem. In Section 3, we describe our methods of discretization for both the adatom diffusion equation and the boundary evolution equation and some implementational details. In Section 4, we present our numerical results.

2. Problem description

Consider the dynamics of adatom islands in an epitaxially growing thin film. An island is a portion of crystal layer that is one atomic layer higher than the adjacent neighboring part of the film surface. Mathematically, we denote by $\Omega \subset \mathbb{R}^2$ the projected domain of the film surface in a two-dimensional Cartesian coordinate system, and assume that Ω is independent of time t. We denote also by $\Omega_0 = \Omega_0(t) \subset \mathbb{R}^2$ the projected domain of the substrate or the exposed film surface with the smallest layer thickness, and by $\Omega_i = \Omega_i(t) \subset \mathbb{R}^2$, $i = 1, \ldots, N$, that of the islands or terraces of relative height i at time t, respectively. Thus, $N + 1$ is the total number of layers that are exposed on the film surface. Note that, since the height of neighboring terraces differs only by one atomic layer,

we conclude that $\overline{\Omega_i(t)} \cap \overline{\Omega_j(t)} = \emptyset$ if and only if $|i-j| \geq 2$. We denote further the corresponding island boundaries by $\Gamma_i(t) = \overline{\Omega_i(t)} \cap \overline{\Omega_{i-1}(t)}$, $i = 1, \ldots, N$.

Denote by $\rho = \rho(x,t)$ the adatom density on Ω. The adatom diffusion on the terraces is described by the diffusion equation for the adatom density

$$\partial_t \rho - D\Delta\rho = F - \tau^{-1}\rho \qquad \text{in } \Omega \backslash \bigcup_{i=1}^{N} \Gamma_i(t) \tag{2.1}$$

where $D > 0$ is the diffusion constant, $F > 0$ is the constant deposition flux rate, and $\tau^{-1} > 0$ is the constant desorption rate. Throughout this paper the unit of length will be the substrate lattice spacing. Thus the deposition rate F denotes the number of atoms deposited per unit time and adsorption site and D is the "hopping rate".

We assume that the adatom density satisfies the following Gibbs-Thomson law on the island boundaries $\Gamma_i(t)$ for $i = 1, \ldots, N$, see [9]:

$$\rho = \rho^*(1 + \frac{\tilde{\gamma}\kappa_i}{k_B T}), \tag{2.2}$$

where κ_i is the curvature of the boundary $\Gamma_i(t)$, ρ^* is a positive constant denoting the thermodynamic equilibrium density at straight steps, k_B is the Boltzmann constant, T is the temperature and $\tilde{\gamma} = \gamma + \gamma_{\theta\theta}$ is the step stiffness of the boundary $\Gamma_i(t)$, related to the orientation-dependent step free energy $\gamma(\theta)$ with θ, $0 \leq \theta \leq 2\pi$, the angle between the outer normal and the x_1-axes.

For the motion of the steps, we assume the following law for the normal velocity v_i of the island boundary $\Gamma_i(t)$ for $i = 1, \ldots, N$ (with the convention that $v_i > 0$ if the movement of Γ_i is in the direction of the unit normal $\vec{n}_i$ pointing from upper to lower terrace)

$$v_i = -D[\nabla\rho \cdot \vec{n}_i]_i + \partial_s(\nu\partial_s(\tilde{\gamma}\kappa_i)), \tag{2.3}$$

where ν is a positive function denoting the (orientation dependent) mobility for migration along edges [9, 5] and ∂_s denotes the tangential derivative along the boundary. For any function $u : \Omega \to \mathbb{R}$, $[u]_i = u^+ - u^-$ denotes the jump of u along $\Gamma_i(t)$ from the upper $(+)$ to the lower $(-)$ terrace. The term $\partial_s\nu(\partial_s(\tilde{\gamma}\kappa_i))$ represents the one-dimensional (in general anisotropic/weighted) "surface" diffusion along the edges.

We assume a flux-free boundary condition for the adatom density on the boundary of the film domain:

$$\frac{\partial\rho}{\partial n} = 0 \qquad \text{at } \partial\Omega \quad \text{for all } t > 0, \tag{2.4}$$

where the normal derivative corresponds to the unit exterior normal $\vec{n}$ to the boundary $\partial\Omega$. We also assume that the initial islands $\Omega_i(0)$ $(i = 0, \ldots, N)$ along with their corresponding boundaries $\Gamma_i(0)$ $(i = 1, \ldots, N)$ are given. Moreover, we assume that the initial adatom density is given by some function $\bar{\rho}$ on Ω. We assume compatibility of this initial value with the boundary condition (2.2), i.e.

$$\bar{\rho}|_{\Gamma_i(0)} = \rho^*(1 + \frac{\tilde{\gamma}\kappa_i}{k_B T}), \tag{2.5}$$

for $i = 1, \dots, N$. Finally, we assume no topological changes in the dynamics, i.e., islands neither nucleate nor coalesce.

3. Variational formulation and finite element discretization

We derive a weak formulation for the time-dependent diffusion equation and use a first order implicit scheme to discretize the time derivative. In each discrete time instant we perform the following steps: (1) we update the discrete boundaries by solving a geometric partial differential equation (PDE) based on the adatom densities and the discrete boundaries from the previous time step; (2) we solve the diffusion equation to update the adatom density using the adatom density from the previous time step and the computed discrete boundaries. In Section 3.1, we describe the weak formulation for the time-dependent diffusion equation and the finite element discretization in each time step. In Section 3.2, we present our algorithm for the geometric PDE of the boundary evolution.

3.1. **Adatom diffusion.**

Assuming the boundaries $\Gamma_i(t)$ to be given, equation (2.1) may be viewed as a standard parabolic PDE with Dirichlet boundary conditions given on the "inner" boundaries $\Gamma_i(t)$ by (2.2). Nevertheless, there are two difficulties, which have to be solved:

(i) Since in the discretization the boundaries $\Gamma_i(t)$ are not part of the 2d-mesh, it is not straight forward how to enforce the Dirichlet boundary conditions (2.2) directly.
(ii) Solving the geometric PDE (2.3) involves the jump of the normal derivative of ρ at the boundaries $\Gamma_i(t)$.

To circumvent both difficulties, a penalty method is used. To this end assume that ρ is smooth inside each Ω_i. Multiplying both sides of the diffusion equation in (2.1) by a smooth, time-independent test function ϕ and integrating by parts, we get

$$\int_\Omega \partial_t \rho\phi + \int_\Omega D\nabla\rho\cdot\nabla\phi + \sum_{i=1}^{N}\int_{\Gamma_i(t)} D[\nabla\rho\cdot\vec{n}_i]_i\phi = \int_\Omega F\phi - \int_\Omega \tau^{-1}\rho\phi. \tag{3.6}$$

We now relax boundary condition (2.2) by a penalty method. More precisely, let $0 < \epsilon = \epsilon(x,t) \ll 1$ be given and replace (3.6) by

(3.7)

$$\int_\Omega \partial_t \rho\phi + \int_\Omega D\nabla\rho\cdot\nabla\phi + \sum_{i=1}^{N}\int_{\Gamma_i(t)} \frac{1}{\epsilon}(\rho - \rho^*(1+\frac{\tilde{\gamma}\kappa_i}{k_BT}))\phi = \int_\Omega F\phi - \int_\Omega \tau^{-1}\rho\phi.$$

Comparing (3.6) and (3.7), one concludes that a solution of (3.7) fulfills the following relaxed boundary condition on $\Gamma_i(t)$:

$$D[\nabla\rho\cdot\vec{n}_i]_i = \frac{1}{\epsilon}(\rho - \rho^*(1+\frac{\tilde{\gamma}\kappa_i}{k_BT})). \tag{3.8}$$

We will use this identity, when solving the geometric PDE (2.3) in Section 3.2, to avoid the evaluation of $\nabla\rho\cdot\vec{n}_i$ at the boundaries $\Gamma_i(t)$.

We would like to mention that in the case of $\nu = 0$, i.e. without surface diffusion, the weak form (3.7) alternatively may be derived by adding a small velocity term in (2.2), giving

$$\rho = \rho^*(1 + \frac{\tilde{\gamma}\kappa_i}{k_B T} + \tilde{\epsilon} v_i). \tag{3.9}$$

Indeed, plugging (2.3) with $\nu = 0$ into (3.9) yields equation (3.8) with $\epsilon = \tilde{\epsilon}\rho^*$, cf. [12].

Now, split the time interval by discrete time instants $0 = t_0 < t_1 < \dots$ and define the time steps $\Delta t_m := t_{m+1} - t_m$ $(m = 0, 1, \dots)$. Using the approximations $\Gamma_i^m \approx \Gamma_i(t_m)$, we have the following formulation of the time discretization problem.

Problem 3.1. *Set $\rho^0 = \bar{\rho}$. For $m = 0, 1, \dots$, find adatom density $\rho^{m+1} \in H^1(\Omega)$ such that*

$$\int_\Omega \frac{\rho^{m+1} - \rho^m}{\Delta t_m}\phi + \int_\Omega D\nabla\rho^{m+1} \cdot \nabla\phi + \sum_{i=1}^N \int_{\Gamma_i^{m+1}} \frac{1}{\epsilon}(\rho^{m+1} - \rho^*(1 + \frac{\tilde{\gamma}\kappa_i^{m+1}}{k_B T}))\phi$$
$$= \int_\Omega F\phi - \int_\Omega \tau^{-1}\rho^{m+1}\phi \qquad \forall \phi_h \in H^1.$$

To discretize in space, let $\mathcal{T}_h^m$ be a conforming triangulation of Ω at time instant t_m. Define the finite element space of globally continuous, piecewise linear elements

$$\mathbb{V}_h^m = \left\{ v_h \in C^0(\overline{\Omega}) \ : \ v_h|_T \in \mathbb{P}^1 \ \ \forall T \in \mathcal{T}_h^m \right\}.$$

Denote by $P_m : C^0(\overline{\Omega}) \to \mathbb{V}_h^m$ the usual Lagrange interpolation operator. With this setting, the space discretization of Problem 3.1 can be summarized as follows:

Problem 3.2. *Let $\rho_h^0 = P_0\bar{\rho}$. For $m = 0, 1, \dots$, determine the discrete adatom density $\rho_h^{m+1} \in \mathbb{V}_h^{m+1}$ by*

$$\int_\Omega \frac{\rho_h^{m+1} - \rho_h^m}{\Delta t_m}\phi_h + \int_\Omega D\nabla\rho_h^{m+1} \cdot \nabla\phi_h + \frac{1}{\epsilon(h)} \sum_{i=1}^N \int_{\Gamma_{i,h}^{m+1}} (\rho_h^{m+1} - \rho^*(1 + \frac{\tilde{\gamma}\kappa_i^{m+1}}{k_B T}))\phi_h$$
$$= \int_\Omega F\phi_h - \int_\Omega \tau^{-1}\rho_h^{m+1}\phi \qquad \forall \phi_h \in \mathbb{V}_h^{m+1}.$$

Here κ_i^{m+1} is the discrete curvatures of $\Gamma_{i,h}^{m+1}$ and $\epsilon(h)$ with $\lim_{h\to 0}\epsilon(h) = 0$ is chosen to be constant on each element and to fulfill $\epsilon(h) = h/D$, which is an optimal choice for linear elements in elliptic problems [6].

In the rest of this subsection, we fix a time step m and drop the subscript and superscript $m + 1$, when no confusion arises. Let $(\phi_k)_{k=1}^L$ be the standard nodal basis of the finite element space $\mathbb{V}_h$, where L is the dimension of $\mathbb{V}_h$. Expand ρ_h as

$$\rho_h^{m+1} = \sum_{k=1}^L r_k\phi_k,$$

for some $R_i = (r_1, \dots, r_L)^t \in \mathbb{R}^L$. Define the following stiffness and mass matrices and load vectors:

$$\begin{array}{llll} \boldsymbol{M} = (M_{kl}), & M_{kl} = (\phi_k, \phi_l)\,; & \boldsymbol{M}^{\Gamma_i} = (M_{kl}^{\Gamma_i}), & M_{kl}^{\Gamma_i} = \langle \phi_k, \phi_l \rangle_{\Gamma_i}; \\ \boldsymbol{A} = (A_{kl}), & A_{kl} = (D\nabla\phi_k, \nabla\phi_l)\,; & \boldsymbol{F} = (F_l), & F_l = (F, \phi_l)\,; \\ \boldsymbol{F}^{\Gamma_i} = (F_l^{\Gamma_i}), & F_l^{\Gamma_i} = \langle \rho^*(1 + \frac{\tilde{\gamma}\kappa_i}{k_B T}), \phi_l \rangle_{\Gamma_i}; & & \end{array}$$

where the index ranges are $1 \le k, l \le L$ and $\langle \cdot, \cdot \rangle_\Gamma$ stands for the L^2 inner product over the current interface Γ whereas $(\cdot, \cdot)$ denotes the L^2 inner product over the domain Ω. The following algorithm is the matrix form of Problem 3.2:

Algorithm 3.1. *For $m = 0, 1, \dots$, find $R^{m+1} \in \mathbb{R}^L$ such that*

$$\begin{aligned} \frac{1}{\Delta t_m} \boldsymbol{M} R^{m+1} + \boldsymbol{A} R^{m+1} + \frac{1}{\epsilon(h)} \sum_{i=1}^{N} \boldsymbol{M}^{\Gamma_i} R^{m+1} + \tau^{-1} \boldsymbol{M} R^{m+1} \\ = \boldsymbol{F} + \frac{1}{\epsilon(h)} \sum_{i=1}^{N} \boldsymbol{F}^{\Gamma_i} + \frac{1}{\Delta t_m} \boldsymbol{M} R^m. \end{aligned}$$

We introduce the following quantities defined on the nodes on the boundaries $\Gamma_{i,h}^{m+1}$:

$$\gamma_i := \frac{1}{\epsilon(h)}(\rho - \rho^*) = \frac{1}{\epsilon(h)}(\rho_h^{m+1}|_{\Gamma_{i,h}^{m+1}} - \rho^*). \tag{3.10}$$

These quantities will enter in the subproblem of the moving boundaries.

As already mentioned in Section 2, the initial adatom density $\bar{\rho}$ (and therefore also the discrete initial adatom density ρ_h^0 in Problem 3.2) has to be compatible with the boundary conditions on the free boundaries Γ_i, see (2.5). Moreover, the accuracy of the values of the adatom density is very important for the evolution of the free boundaries, see (3.10). Therefore we solve a separate problem to calculate suitable initial values ρ_h^0. As in [12] we substitute the discrete time derivative in Problem 3.2 by $\rho_{t,h}^0 = 0$. We eventually arrive at the following problem to determine ρ_h^0.

Problem 3.3. *For given initial polygonal curves $\Gamma_{i,h}^0$, $i = 1, \dots, N$ determine the initial discrete adatom density $\rho_h^0 \in \mathbb{V}_h^0$ as the solution of*

$$\int_\Omega D\nabla\rho_h^0 \cdot \nabla\phi_h + \frac{1}{\epsilon(h)} \sum_{i=1}^{N} \int_{\Gamma_i^0} (\rho_h^0 - \rho^*(1 + \frac{\tilde{\gamma}\kappa_i^0}{k_B T}))\phi_h = \int_\Omega F\phi_h - \int_\Omega \tau^{-1}\rho_h^0\phi$$

for all $\phi_h \in \mathbb{V}_h^0$, with notations as in Problem 3.2.

Using the nodal basis and the mass and stiffness matrices as above, Problem 3.3 yields the following algorithm for the initial value:

Algorithm 3.2. *Find $R^0 \in \mathbb{R}^L$ such that*

$$\boldsymbol{A} R^0 + \frac{1}{\epsilon(h)} \sum_{i=1}^{N} \boldsymbol{M}^{\Gamma_i} R^0 + \tau^{-1} \boldsymbol{M} R^0 = \boldsymbol{F} + \frac{1}{\epsilon(h)} \sum_{i=1}^{N} \boldsymbol{F}^{\Gamma_i}.$$

3.2. **Boundary evolution.** Now assuming the adatom density ρ to be given, we use the identity (3.8) to avoid the direct evaluation of $\nabla\rho\cdot\vec{n}_i$ at the boundaries $\Gamma_i(t)$ in the velocity law in (2.3). Thus we get the following geometric PDE for the boundary evolution of the moving boundaries Γ_i, $i=1,\dots,N$:

$$v_i = \frac{1}{\epsilon}(\rho-\rho^*) - \frac{1}{\epsilon}\rho^*\frac{\tilde{\gamma}\kappa_i}{k_BT} + \partial_s(\nu\partial_s(\tilde{\gamma}\kappa_i)). \tag{3.11}$$

This equation can be interpreted as an equation for (weighted/anisotropic) surface diffusion with lower order terms if $\nu>0$ or for the (weighted/anisotropic) mean curvature flow with a forcing term if $\nu=0$. A variational formulation and discretization by parametric finite elements for such a highly nonlinear 4th order ($\nu>0$) or 2nd order ($\nu=0$) equation was given in [1] (for the isotropic case, i.e. $\nu=const$ and $\gamma=const$). We will now recall this formulation and modify it to also handle anisotropy.

By introducing the position vector $\vec{x}_i$, the curvature vector $\vec{\kappa}_i$, and the velocity vector $\vec{v}_i$, a system of equations for $\vec{\kappa}_i$, κ_i, v_i, and $\vec{v}_i$ can be derived. By the geometric identity $\vec{\kappa}_i=-\partial_{ss}\vec{x}_i$, the velocity law (3.11), and the relations between the vector valued and scalar quantities $\kappa_i=\vec{\kappa}_i\cdot\vec{n}_i$ and $\vec{v}_i=v_i\vec{n}_i$, we obtain

$$\vec{\kappa}_i = -\partial_{ss}\vec{x}_i, \tag{3.12}$$

$$\kappa_i = \vec{\kappa}_i\cdot\vec{n}_i, \tag{3.13}$$

$$v_i = f_i, \tag{3.14}$$

$$\vec{v}_i = v_i\vec{n}_i, \tag{3.15}$$

where

$$f_i := \frac{1}{\epsilon}(\rho-\rho^*) - \frac{1}{\epsilon}\rho^*\frac{\tilde{\gamma}\kappa_i}{k_BT} + \partial_s(\nu\partial_s(\tilde{\gamma}\kappa_i))$$

Consider the discrete time instant t_m and time step $\Delta t_m := t_{m+1}-t_m$ as in Section 3.1. We represent the next free boundary Γ_i^{m+1} in terms of the current boundary Γ_i^m by updating the position vectors

$$\vec{x}_i \leftarrow \vec{x}_i + \Delta t_m\vec{v}_i. \tag{3.16}$$

The time discretization assumes that all geometric quantities such as $\vec{n}_i$, ∂_s are evaluated on the *current* free boundaries Γ_i^m. In contrast to the geometric quantities, the unknowns $\vec{\kappa}_i$, κ_i, v_i, $\vec{v}_i$ are treated implicitly. In particular, in view of (3.16), we define

$$\vec{\kappa}_i^{m+1} := -\partial_{ss}(\vec{x}_i^m + \Delta t_m\vec{v}_i^{m+1}). \tag{3.17}$$

To derive a weak formulation, we first write the above equations in terms of the weighted curvature

$$\tilde{\kappa}_i := \tilde{\gamma}\kappa_i, \tag{3.18}$$

and then proceed similarly as in [7]: multiply (3.13), (3.14), (3.15), and (3.17) by test functions $\vec{\psi}\in\vec{H}^1(\Gamma_i)$ and $\psi\in H^1(\Gamma_i)$, and use integration by parts for the operator ∂_s. For simplicity we have hereafter dropped the superscript $m+1$ for the unknowns. Furthermore, using the notation $\langle\cdot,\cdot\rangle$ for the L^2 inner product over the current interfaces Γ_i^m, we arrive at the following semi-implicit, time discrete set of equations:

Problem 3.4. *For $m = 1, 2, \ldots$ find $\vec{\kappa}_i \in \vec{H}^1(\Gamma_i^m)$, $\tilde{\kappa}_i \in H^1(\Gamma_i^m)$, $v_i \in H^1(\Gamma_i^m)$, and $\vec{v}_i \in \vec{H}^1(\Gamma_i^m)$ such that*

$$\begin{aligned}
\langle \vec{\kappa}_i, \vec{\psi} \rangle - \Delta t_m \langle \partial_s \vec{v}_i, \partial_s \vec{\psi} \rangle &= \langle \partial_s \vec{x}_i^m, \partial_s \vec{\psi} \rangle && \forall \vec{\psi} \in \vec{H}^1(\Gamma_i^m), \\
\langle \tilde{\kappa}_i, \psi \rangle - \langle \tilde{\gamma} \vec{\kappa}_i \cdot \vec{n}_i, \psi \rangle &= 0 && \forall \psi \in H^1(\Gamma_i^m), \\
\langle v_i, \psi \rangle + \langle \alpha \partial_s \tilde{\kappa}_i, \partial_s \psi \rangle + \beta \langle \tilde{\kappa}_i, \psi \rangle &= \langle \gamma_i, \psi \rangle && \forall \psi \in H^1(\Gamma_i^m), \\
\langle \vec{v}_i, \vec{\psi} \rangle - \langle v_i \vec{n}_i, \vec{\psi} \rangle &= 0 && \forall \vec{\psi} \in \vec{H}^1(\Gamma_i^m).
\end{aligned}$$

where we have used the following abbreviations:

$$\alpha = \nu; \quad \beta = \frac{1}{\epsilon} \frac{\rho^*}{k_B T}; \quad \gamma_i = \frac{1}{\epsilon}(\rho - \rho^*).$$

Note that in the above formulation the adatom density ρ is needed only for computing γ_i. The discrete scheme can be written as a matrix-vector system by using a nodal bases as usual, and is solved by a Schur complement approach, see [1] for details. Note that in contrast to [1] in the case of anisotropy, i.e. $\tilde{\gamma}$ and/or ν not being constant, we solve for the unknowns $\tilde{\kappa}_i, \vec{\kappa}_i, v_i, \vec{v}_i$ rather than for $\kappa_i, \vec{\kappa}_i, v_i, \vec{v}_i$.

The subproblem of boundary evolution consists of solving N decoupled problems for each interface $\Gamma_{i,h}$, $i = 1, \ldots, N$. For the adatom diffusion problem the new interfaces $\Gamma_{i,h}^{m+1}$ and their weighted curvatures $\tilde{\kappa}_{i,h}$ will enter.

3.3. **Implementation.** The numerical method is implemented using ALBERT, an adaptive finite element software for scientific computation [13]. The program for the two dimensional adatom diffusion and that for the one dimensional boundary evolution are coupled via TCP/IP. The matrices are assembled using the standard assembling tools of ALBERT except for the matrices involving line integrals. For the latter see [1].

Adaptivity for adatom diffusion. To obtain satisfactory computational results, a mesh with a sufficiently fine resolution near the moving island boundaries is needed. Thus it is indispensable to use some adaptive strategy for local mesh refinement and coarsening. As described in [1] we use an L^2-like error indicator for local mesh coarsening and a purely geometric criterion for refinement, ensuring the mesh size of the 2d grid at the moving boundaries to be at least as fine as the 1d mesh size.

Adaptivity for boundary evolution. The 1d finite element meshes for the boundaries are also adapted. Nodes are inserted or removed from the current mesh in each time step according to the criterion that the distance between neighboring nodes is almost a constant.

Algorithm. Combining the methods described so far we arrive at the following algorithm.

Algorithm 3.3. *Let the initial boundaries $\Gamma_{i,h}^0$ be given. Set $m = 0$.*

(1) *compute curvature $\kappa_{i,h}^0$ of the initial boundaries*
(2) *compute initial adatom density ρ_h^0*
  (a) *compute ρ_h^0*
  (b) *compute $\gamma_i = \gamma_i(\rho_h^0)$*
(3) *compute free boundaries $\Gamma_{i,h}^{m+1}$ and curvatures $\kappa_{i,h}^{m+1}$*
  (a) *compute $v_{i,h}^{m+1}$, $\vec{v}_{i,h}^{m+1}$ and $\Gamma_{i,h}^{m+1}$*
  (b) *refine and coarse $\Gamma_{i,h}^{m+1}$*
  (c) *compute $\kappa_{i,h}^{m+1}$ on $\Gamma_{i,h}^{m+1}$*
(4) *compute adatom density ρ_h^{m+1}*
  (a) *refine and coarse $\mathcal{T}_h^m$*
  (b) *compute ρ_h^{m+1}*
  (c) *compute $\gamma_i = \gamma_i(\rho_h^{m+1})$*
(5) *set $m := m + 1$, go to 3*

4. Numerical results

We first present numerical results for the geometric motion of curves in Section 4.1. In Section 4.2 we then investigate numerically the isotropic growth of a single circular island, and compare the numerical results with the known analytical solutions. The influence of 1-dimensional surface diffusion on the anisotropic growth of a single island is shown in Section 4.3. Further examples are the evolution of a "wedding cake" and the anisotropic evolution of several islands are shown in Section 4.4 and Section 4.5, respectively.

Anisotropies will be described in terms of a function $f(\theta)$, $0 \le \theta \le 2\pi$, such that

$$\tilde{\gamma}(\theta) = \gamma_0(f(\theta) + f''(\theta)), \tag{4.19}$$

where we consider anisotropies of the type

$$f(\theta) = 1.0 + A\cos(k\theta)$$

with A being the strength of the anisotropy and k the periodicity. Thus, for $\tilde{\gamma}$ to be positive, it is necessary that $(k^2 - 1)A < 1$.

Unless otherwise stated, we use the following data in all numerical simulations:

- parameters: $D = 10^5,\ F = 1,\ \rho^* = 10^{-4},\ \tau^{-1} = 0,\ \tilde{\gamma} = \gamma_0 = 0.3,$ $\nu = 10,\quad k_B T = 1;$
- domain: Ω is a circular domain with radius 10;
- mesh size of the initial 1d finite element mesh: $h \approx 0.05$;
- time step: 10^{-4}.

4.1. **Geometric motion of curves.** Our first test example is the purely geometric motion of curves governed by Problem 3.4 in Section 3.2, decoupled from the adatom diffusion. Considering a single curve Γ we may write equation (3.11) as

$$v = \gamma_i - \beta \frac{\tilde{\gamma}\kappa_i}{k_B T} + \partial_s(\nu \partial_s(\tilde{\gamma}\kappa_i)), \tag{4.20}$$

where γ_i is a function on the curve Γ, $\beta \geq 0$ is a constant and $\tilde{\gamma}, \nu$ are positive functions of a single variable $0 \leq \theta \leq 2\pi$ denoting the angle of the outer normal of Γ with the x_1-axis.

Choosing $\tilde{\gamma}$, ν, β and γ_i in a suitable way, equation (4.20) and therefore the algorithm described in Section 3.2 can be used to describe several geometric evolution equations.

We will consider the following two examples:

- weighted mean curvature flow: $\nu = 0$, $\beta \neq 0$, $\tilde{\gamma} \neq 0$ and $\gamma_i = 0$;
- weighted surface diffusion: $\nu = 1$, $\beta = 0$, $\tilde{\gamma} \neq 0$ and $\gamma_i = 0$.

The smoothing properties of the mean curvature flow and of the surface diffusion have already been presented in [1] for the isotropic case. Here we will give some examples of anisotropic flows.

For the anisotropic surface free energy $A_\gamma(\Gamma) = \int_\Gamma \gamma$ the corresponding Wulff shape $\mathcal{W}_\gamma$

$$\mathcal{W}_\gamma = \{\vec{x} \in \mathbb{R}^2 \,|\, \vec{x} \cdot \vec{n} \leq \gamma(\vec{n}(\theta)), \forall \vec{n} \in \mathbb{R}^2, |\vec{n}| = 1\}.$$

is associated. The weighted curvature $\tilde{\kappa} = \tilde{\gamma}$ is constant on $\mathcal{W}_\gamma$ and the Wulff shape minimizes the 1d-surface free energy under the constraint of fixed area. Therefore, $\mathcal{W}_\gamma$ describes the equilibrium shape in the case of anisotropy. For this reason one expects the surface diffusion flow to tend to the Wulff shape as a stationary solution and the mean curvature flow to shrink a given curve towards the (rescaled) Wulffshape. Our numerical experiments agree perfectly with these both expectations as can be seen in Figure 1 and Figure 2. We have chosen two different anisotropies f with periodicity 3 and 6. The corresponding Wulff shapes are depicted in Figure 1.

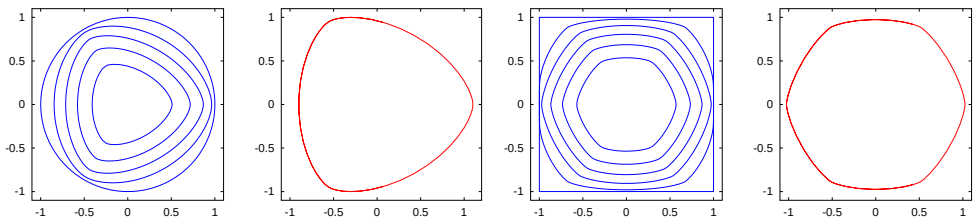

FIGURE 1. *Anisotropic mean curvature flow: starting with a circle and anisotropy* $f(\theta) = 1.0 + 0.1\cos(3\theta)$*; snapshots at* $t = 0.0$, $t = 0.1$, $t = 0.2$, $t = 0.3$, $t = 0.4$ *and corresponding Wulff shape (left); starting with a square and anisotropy* $f(\theta) = 1.0 + 0.025\cos(6\theta)$*; snapshots at* $t = 0.0$, $t = 0.1$, $t = 0.2$, $t = 0.3$, $t = 0.4$, $t = 0.5$ *and corresponding Wulff shape (right).*

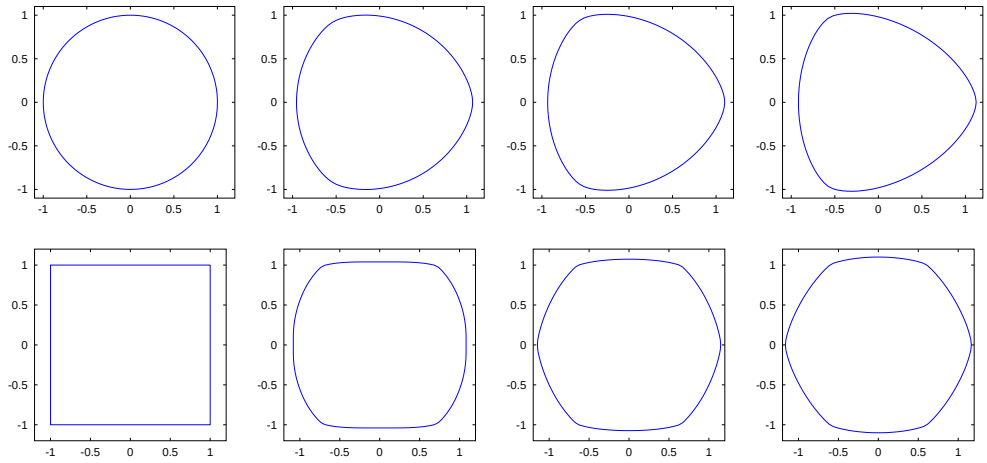

FIGURE 2. *Anisotropic surface diffusion: starting with a circle and anisotropy* $f(\theta) = 1.0 + 0.1\cos(3\theta)$ *(first row); starting with a square and anisotropy* $f(\theta) = 1.0 + 0.025\cos(6\theta)$ *(second row); snapshots at* $t = 0.0$, $t = 0.01$, $t = 0.02$, $t = 0.1$.

4.2. **Growth of a single circular island.** We consider a single, circular island $\Omega_1(t)$ of radius $R(t)$ at time t that is growing on a terrace which is a concentric circular region with radius R_Ω. In the quasi-stationary approximation for the adatom diffusion, the time dependence in the diffusion equation (2.1) is dropped. This approximation is valid if $F/D \ll 1$. Since $F/D = 10^{-5} \ll 1$, we expect our simulation of the time dependent diffusion equation to be in good agreement with the analytic solution of the quasi-stationary diffusion equation.

Using polar coordinates (r, θ) with the origin at the center of the circular island, the radially symmetric solution of the quasi-stationary diffusion equation is given by [10]

$$\rho_1(r,t) = \frac{F}{4D}\left(R(t)^2 - r^2\right) + \rho^*\left(1 + \frac{\tilde{\gamma}}{k_B T R(t)}\right),$$
$$\rho_0(r,t) = \frac{F}{4D}\left(R(t)^2 - r^2\right) + \frac{FR_\Omega^2}{2D}\ln\left(\frac{r}{R(t)}\right) + \rho^*\left(1 + \frac{\tilde{\gamma}}{k_B T R(t)}\right).$$

Since the curvature $\kappa_1 = 1/R(t)$ of the circular boundary $\Gamma_1(t)$ is spatially constant, we have $\partial_{ss}\kappa_1 = 0$. Furthermore, since the velocity of the circular boundary $\Gamma_1(t)$ is given by $v_1 = R'(t)$, by a simple calculation we get $R'(t) = FR_\Omega^2/(2R(t))$, i.e., $(R(t)^2)' = FR_\Omega^2$. Thus, we obtain the dynamic law

$$R(t)^2 = FR_\Omega^2 t + R(0)^2 \tag{4.21}$$

for the evolution of the circular boundary $\Gamma_1(t)$.

For the simulation we have chosen an island with initial radius $R(0) = 3.0$ growing on a terrace of radius $R_\Omega = 10.0$. From Figure 3, showing the adaptively refined 2d mesh, the computed 1d boundary $\Gamma_{1,h}$, and the computed adatom density ρ_h at various times, it can be seen that the evolution of the growing island is very stable.

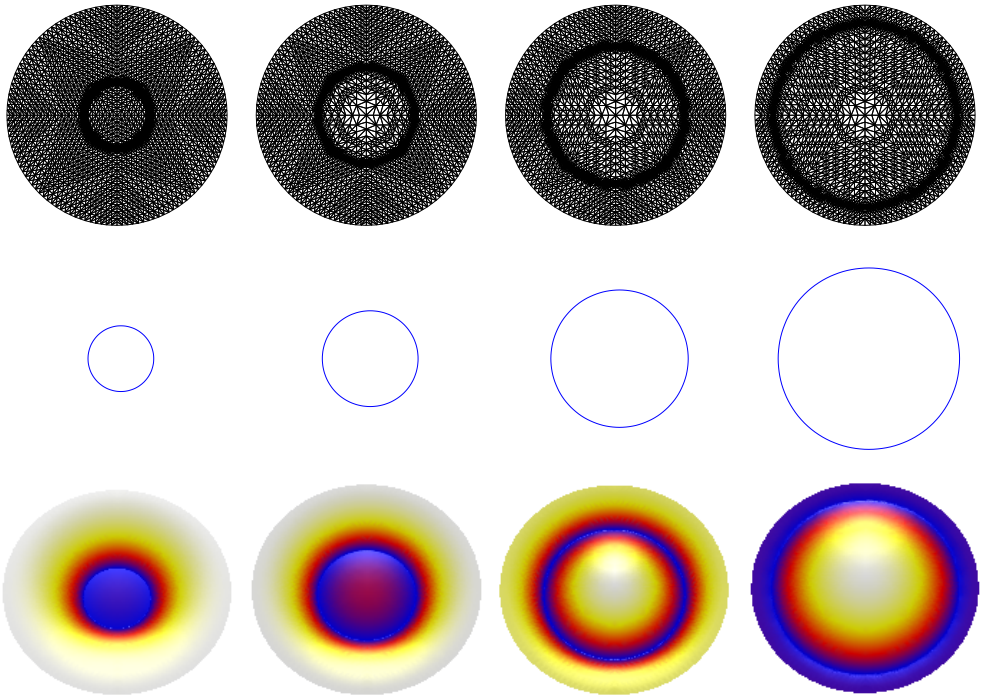

FIGURE 3. *2d mesh, 1d boundary, and adatom density at time instants* $t = 0.0, 0.1, 0.3, 0.6$.

As a test of mass conservation, the growth rate of the island area is depicted in Figure 4 (right picture). Evaluating equation (4.21), one expects a growth rate of $F|\Omega| \approx 314.15$. The simulations are in good agreement with this value, as shown by a least square fit of the numerical data, see Figure 4 (right picture). Figure 4 (left) shows the profile of the adatom density at the same time instants as in Figure 3.

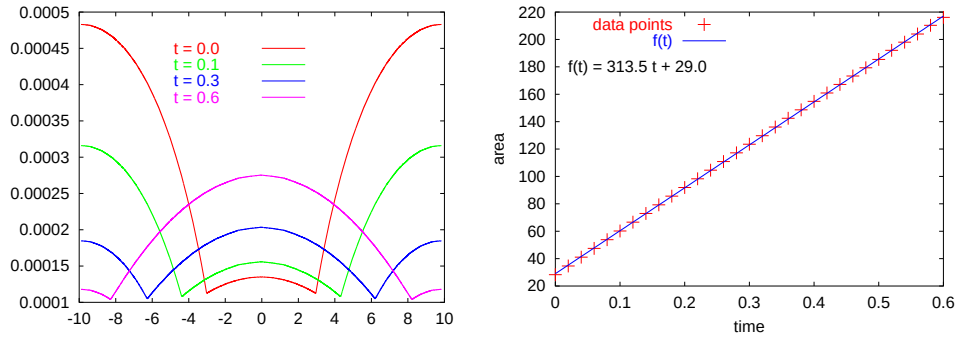

FIGURE 4. *Adatom density profile of the numerical solution (left picture) and area growth rate (right picture). The function f is a least square fit of the data to an affine linear function.*

Finally, in Figure 5, the numerical and analytical solutions are compared by depicting the relative error of the adatom density along the x_1-axis for the same time instants as in Figure 4. The maximum relative pointwise error is less then 2% over the whole time period. We conclude that the numerical algorithm is fairly accurate for describing both, the free boundary evolution and the adatom diffusion equation.

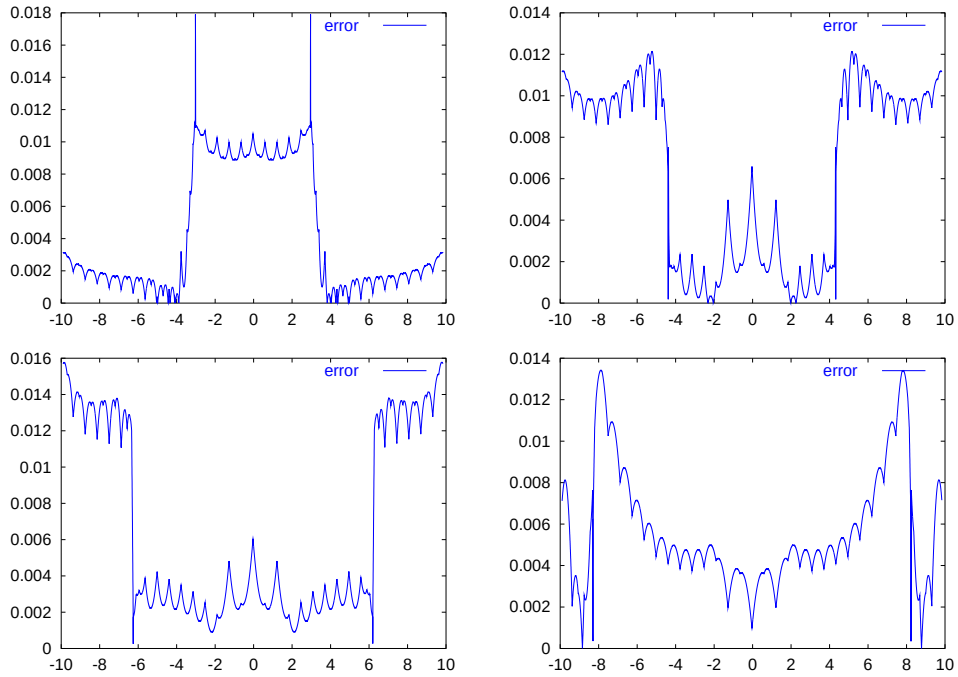

FIGURE 5. *Relative pointwise error of the numerical solution at time instants* $t = 0.0,\ 0.1,\ 0.3,\ 0.6$.

4.3. **Anisotropic growth of a single island.** In this example we investigate the influence of the 1-dimensional surface diffusion on anisotropic growth. We simulate the anisotropic growth of a single island with anisotropy given by

$$f(\theta) = 1.0 + 0.1\cos 3\theta,$$

both without surface diffusion (i.e. $\nu = 0$) and with surface diffusion ($\nu = 10.0$) and compare the respective results. Starting with a circle, we expect the island to at least resemble the corresponding Wulff shape (see Figure 1) in both cases. The simulated evolutions of the moving boundaries are shown in Figure 6. Comparing the two figures, it is seen that surface diffusion drives the evolution of the boundary towards the Wulff shape.

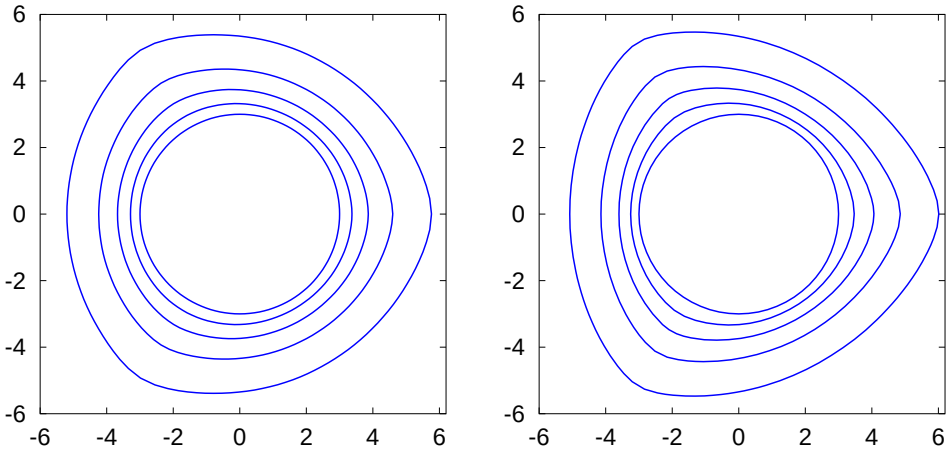

FIGURE 6. *Anisotropic growth of a single island with anisotropy* $f(\theta) = 1.0 + 0.1\cos 3\theta$. *Moving boundary at time instants* $t = 0.0, 0.02, 0.05, 0.1, 0.2$ *(from inner to outer curve). Left: without surface diffusion; right: with surface diffusion.*

4.4. **Evolution of a wedding cake.** The next example is a growing "wedding cake". We consider three circular islands with radii $R(1) = 7.0$, $R(2) = 5.0$, $R(3) = 3.0$ sitting on top of each other and growing on a circular substrate of radius $R_\Omega = 10.0$.

As in the case of one circular island, see Figure 4 (right picture), we have calculated the area growth rate using a least square fit yielding a growth rate of 316.8, which again is in good agreement with the expected value $F|\Omega| \approx 314.4$. In Figure 7 we show the discrete height function at various times. The discrete height function was obtained by marking the elements of the 2d-mesh by the height, i.e. the index i (number of atomic layers) of the corresponding terrace. If the boundary Γ_i intersects the element, it is marked by $i + \frac{1}{2}$.

The adatom density profile is represented in Figure 8.

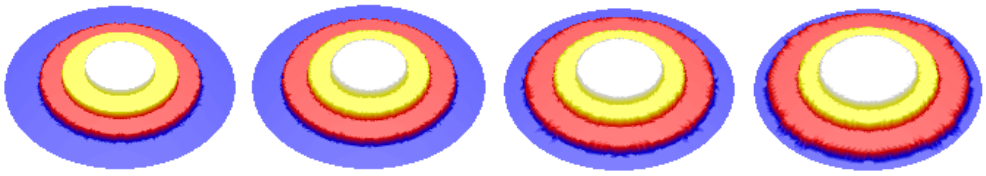

FIGURE 7. *Discrete height function of the wedding cake at time instants* $t = 0.0, 0.1, 0.3, 0.5$.

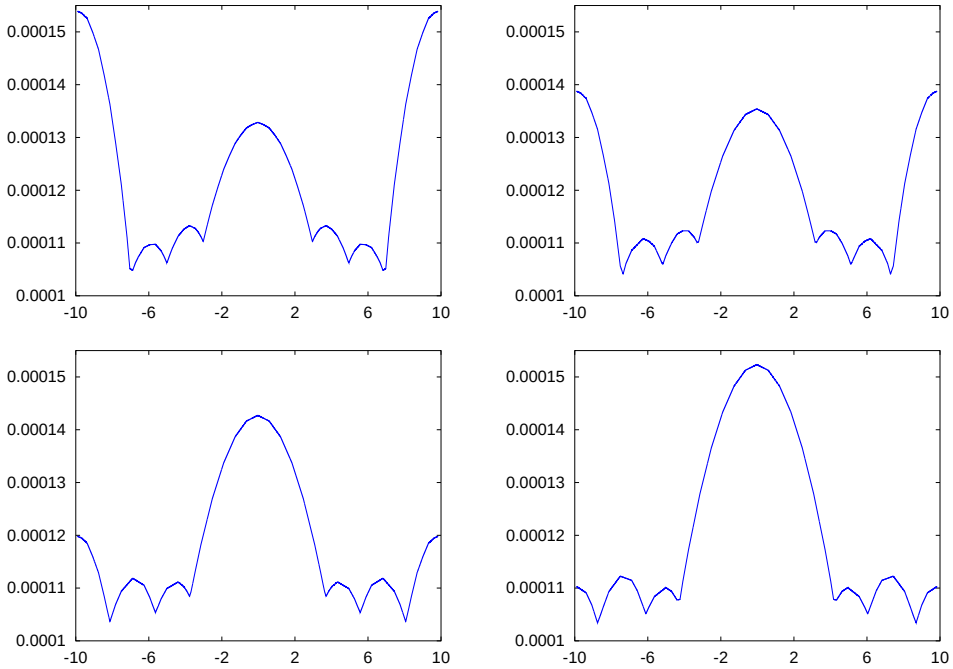

FIGURE 8. *Adatom density profile of the wedding cake on a cut along the x_1-axis at times $t = 0.0$, 0.1, 0.3, 0.5.*

4.5. **Anisotropic growth.** We finally present the simulation of the anisotropic growth of several islands on a rectangular substrate of length 80 and width 40. The initial configuration is shown in Figure 9. The island boundaries at various times are represented in Figure 10. We observe that the shapes of the two small islands very quickly resemble the Wulff shape. However, as soon as the islands get close to the boundaries (either of the substrate or of another island), the growth velocity of that part of the island boundary decreases rapidly. Noting that the total area growth rate for the quasistationary solution is $F|\Omega| = 800.0$, we conclude that the value 792.6 obtained from the simulation is fairly good. Figure 11 illustrates our adaptive refinement and coarsening strategies.

FIGURE 9. *Anisotropic growth: initial configuration of the three circular islands on a rectangular substrate, depicted as the discrete height function.*

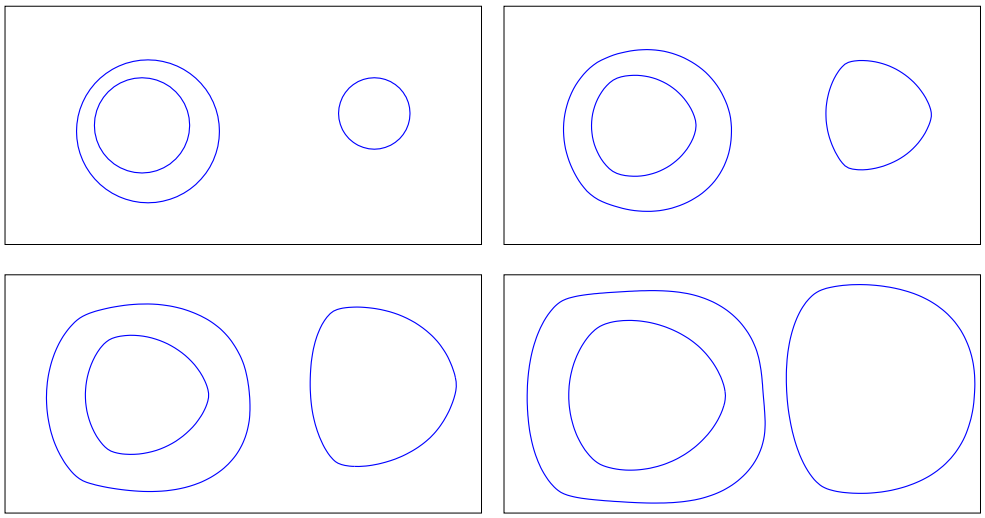

FIGURE 10. *Anisotropic growth: Island boundaries at times* $t = 0.0$, $t = 0.1$, $t = 0.3\, t = 0.6$.

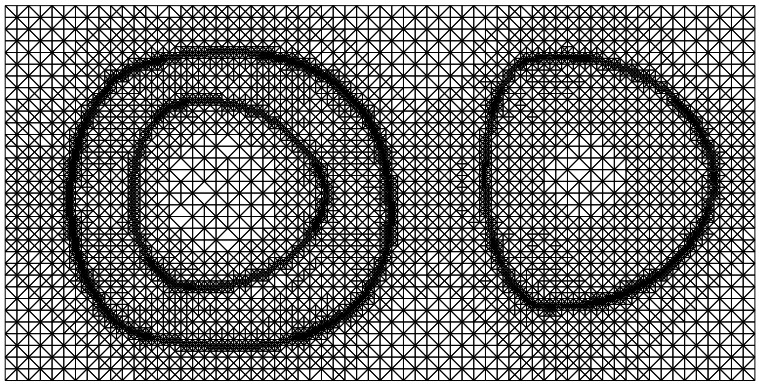

FIGURE 11. *Anisotropic growth: Adaptively refined mesh at time* $t = 0.3$.

References

1. E. Bänsch, F. Haußer, O. Lakkis, B. Li, and A. Voigt, *Finite element method for epitaxial growth with attachment-detachment kinetics*, Preprint No. 70, SFB 611, Universität Bonn (2003), submitted.
2. E. Bänsch, P. Morin, and R. H. Nochetto, *Finite element methods for surface diffusion*, Proceedings of International Conference on Free Boundary Problems: Theory and Applications, Trento, 2002 (to appear).
3. W. K. Burton, N. Cabrera, and F. C. Frank, *The growth of crystals and the equilibrium of their surfaces*, Phil. Trans. Roy. Soc. London Ser. A **243** (1951), no. 866, 299–358.
4. R. E. Caflisch, W. E, M. F. Gyure, B. Merriman, and C. Ratsch, *Kinetic model for a step edge in epitaxial growth*, Phys. Rev. E **59** (1999), no. 6, 6879–6887.
5. R. E. Caflisch and B. Li, *Analysis of island dynamics in epitaxial growth of thin films*, Multiscale Model. Simul. **1** (2003), no. 1, 150–171.
6. P.G. Ciarlet, *The finite element method for elliptic problems*, North-Holland, 1976.
7. G. Dziuk, *An algorithm for evolutionary surfaces*, Numer. Math. **58-6** (1991), 603–611.
8. R. Ghez and S. S. Iyer, *The kinetics of fast steps on crystal surfaces and its application to the molecular beam epitaxy of silicon*, IBM J. Res. Develop. **32** (1988), 804–818.
9. J. Krug, *Four lectures on the physics of crystal growth*, Physica A **318** (2002), 47–82.
10. B. Li, A. Rätz, and A. Voigt, *Stability of a circular epitaxial island*, Preprint No. 50, SFB 611, Universität Bonn (2002 (submitted)).
11. A. Pimpinelli and J. Villain, *Physics of crystal growth*, Cambridge University Press, Cambridge, 1998.
12. A. Schmidt, *Computation of three dimensional dendrites with finite elements*, J. Comp. Physics **125** (1996), 293–312.
13. A. Schmidt and K. G. Siebert, *Albert - software for scientific computations and applications*, Acta Math. Univ. Comenianae **70** (2001), 105–122.

Eberhard Bänsch, Numerical Mathematics and Scientific Computing, WIAS, Mohrenstrasse 39, 10117 Berlin, Germany

E-mail address: baensch@wias-berlin.de

Frank Hausser, Crystal Growth Group, Research Center caesar, Ludwig-Erhard-Allee 2, 53175 Bonn, Germany

E-mail address: hausser@caesar.de

Axel Voigt, Crystal Growth Group, Research Center caesar, Ludwig-Erhard-Allee 2, 53175 Bonn, Germany

E-mail address: voigt@caesar.de